

RESEARCH LETTER

10.1002/2014GL061121

Key Points:

- We analyzed data of radiative forcing and temperature from the last 800,000 years
- The equilibrium climate sensitivity depends on the background climate state
- Equilibrium climate sensitivity is higher in warmer than in colder climates

Supporting Information:

- Readme
- Text S1

Correspondence to:

A. S. von der Heydt,
a.s.vonderheydt@uu.nl

Citation:

von der Heydt, A. S., P. Köhler, R. S. W. van de Wal, and H. A. Dijkstra (2014), On the state dependency of fast feedback processes in (paleo) climate sensitivity, *Geophys. Res. Lett.*, 41, 6484–6492, doi:10.1002/2014GL061121.

Received 8 JUL 2014

Accepted 19 AUG 2014

Accepted article online 22 AUG 2014

Published online 17 SEP 2014

On the state dependency of fast feedback processes in (paleo) climate sensitivity

A. S. von der Heydt¹, P. Köhler², R. S. W. van de Wal¹, and H. A. Dijkstra¹

¹Institute for Marine and Atmospheric Research Utrecht, Utrecht University, Utrecht, Netherlands,

²Alfred-Wegener-Institut, Helmholtz-Zentrum für Polar- und Meeresforschung, Bremerhaven, Germany

Abstract Paleo data have been frequently used to determine the equilibrium (Charney) climate sensitivity S^a , and—if slow feedback processes (e.g., land-ice albedo) are adequately taken into account—they indicate a similar range as estimates based on instrumental data and climate model results. Many studies assume the (fast) feedback processes to be independent of the background climate state, e.g., equally strong during warm and cold periods. Here we assess the dependency of the fast feedback processes on the background climate state using data of the last 800 kyr and a box model of the climate system for interpretation. Applying a new method to account for background state dependency, we find $S^a = 0.61 \pm 0.07 \text{ K (W m}^{-2}\text{)}^{-1}$ ($\pm 1\sigma$) using a reconstruction of Last Glacial Maximum (LGM) cooling of -4.0 K and significantly lower climate sensitivity during glacial climates. Due to uncertainties in reconstructing the LGM temperature anomaly, S^a is estimated in the range $S^a = 0.54\text{--}0.95 \text{ K (W m}^{-2}\text{)}^{-1}$.

1. Introduction

The Charney climate sensitivity S^a is determined by fast feedbacks, i.e., those with a response time scale faster than a typical forcing time scale (usually taken as ~ 100 years for the anthropogenic CO_2 increase [Charney, 1979; Knutti and Hegerl 2008; Rohling et al., 2012]). Recently, a systematic approach has been proposed to determine S^a from paleoclimate data by correcting the values of the specific climate sensitivity $S_{[\text{CO}_2]}$ caused by the radiative forcing of atmospheric CO_2 changes for the slow feedbacks such as land-ice albedo [Rohling et al., 2012]. This approach has revealed values of S^a within a range of $0.6\text{--}1.3 \text{ K (W m}^{-2}\text{)}^{-1}$ at the 68% probability level for the last 65 million years, which is similar to the range estimated from the Coupled Model Intercomparison Project Phase 5 climate model ensemble [Vial et al., 2013]. There are, however, several assumptions made in order to determine the estimates of S^a from paleo records. One of them is that the strength of the fast feedbacks is independent of the background state of the climate system. Many studies mention that this assumption may be unrealistic [Senior and Mitchell, 2000; Crucifix, 2006; Andrews and Forster, 2008; Yoshimori et al., 2011], but the effect of the background state dependency on the values of S^a has been estimated only for the Last Glacial Maximum (LGM) and present day.

Climate sensitivity is determined from the radiation balance of the Earth by $S = \frac{\Delta T}{\Delta R}$, where ΔT is the global mean temperature change and ΔR is the change in radiative forcing between two “equilibrium” states. Here equilibrium means that those processes faster than the original forcing time scale (e.g., CO_2 increase) are in equilibrium with the global mean surface temperature (GMST). (The different terms in the radiation balance and how they enter the climate sensitivity are explicitly written out in Text S1 in the supporting information.) In paleoclimate studies, equilibrium states are compared with, e.g., different land ice distributions. The slow land-ice albedo feedback is in this case considered as additional forcing. To indicate which processes (with subscripts X, Y, \dots) are considered a forcing, the specific climate sensitivities $S_{[X,Y,\dots]}$ have been defined [Rohling et al., 2012]:

$$S_{[\text{CO}_2]} = \frac{\Delta T}{\Delta R_{[\text{CO}_2]}}, \tag{1}$$

$$S_{[\text{CO}_2,LI]} = \frac{\Delta T}{\Delta R_{[\text{CO}_2]} + \Delta R_{[LI]}}. \tag{2}$$

Here $\Delta R_{[\text{CO}_2]}$ and $\Delta R_{[LI]}$ are, respectively, the radiative forcing contributions of CO_2 and of surface albedo changes caused by land-ice (LI). The specific climate sensitivity $S_{[\text{CO}_2]}$ can be derived from paleo data by

using reconstructed values for ΔT and $\Delta R_{[\text{CO}_2]}$. To estimate the Charney sensitivity S^a , the values of $S_{[\text{CO}_2]}$ need to be corrected for all slow feedback processes or forcings other than CO_2 [Rohling *et al.*, 2012]. Therefore, reconstructions of land-ice area and other slow processes are necessary as well.

In this paper, we estimate the background state dependency by analyzing paleoclimate data from the glacial-interglacial transitions during the Late Pleistocene [Köhler *et al.*, 2010]. In the latter work, S^a was calculated from the Last Glacial Maximum (LGM) part of these data and corrected for state dependency based on a single climate model. However, it has been argued that such corrections are highly model dependent [Crucifix, 2006]. Here we suggest a new method for estimating climate sensitivity from paleo data in order to account for background state dependency of the fast feedbacks.

2. Methods to Estimate Climate Sensitivity

To illustrate different methods to estimate climate sensitivity, we make use of a conceptual box model of the climate system [Gildor and Tziperman, 2001; Gildor *et al.*, 2002], which has been shown to simulate the glacial-interglacial transitions. The atmosphere is represented by four meridional boxes, the ocean component consists of two layers of four meridional boxes each. The model includes land-ice, sea-ice, and a carbon cycle model such that atmospheric CO_2 concentration is a prognostic variable in the model. The model contains one dynamic fast feedback, namely, the sea ice-albedo feedback, and one slow feedback, the land-ice albedo feedback. On fast to intermediate time scales, there is an additional process in the radiative balance due to heat exchange between ocean and atmosphere. All other fast feedbacks (water vapor, clouds, aerosols, and lapse rate) are represented by a fixed temperature response to the radiative forcing in the system. The simulated glacial-interglacial cycles show a peak-to-peak global mean temperature difference of 3.2 K (Figure 1a). Corresponding CO_2 differences are about 50 ppmv which are here completely generated by the effect of the solubility pump in the ocean. In this model the fast sea ice feedback is responsible for the abrupt glacial-interglacial variations—the so-called sea ice switch mechanism as suggested by Gildor and Tziperman [2001]. The sea ice cover changes in the model are about 1.5 times larger than suggested by proxy data Köhler *et al.* [2010], while Northern Hemisphere land ice cover changes are smaller (Figure 1b). Nevertheless, for our purpose of investigating a potential background state dependency of the fast feedbacks, this model is very illustrative.

To determine the interglacial (“present-day”) value of S^a from the box model, we directly compute it by doubling CO_2 (without the carbon cycle model) starting at a peak interglacial state and integrating the model for 100 years as is usually done with climate models (Figures 1c and 1d). The glacial value of the same climate sensitivity (but with a different background state) was determined in a similar way, initializing the model from a peak glacial state.

The glacial and interglacial values for $S_{[\text{CO}_2]}$ are not the same, as expected, due to different land-ice distributions. The Charney sensitivity S^a can be approximated as $S_{[\text{CO}_2, \text{LI}]}$ where the radiative forcing due to land ice changes $\Delta R_{[\text{LI}]}$ is considered (equation (2)). In the $2 \times \text{CO}_2$ experiments, however, the values for $S_{[\text{CO}_2, \text{LI}]}$ remain almost the same as for $S_{[\text{CO}_2]}$ (blue and red bars in Figure 1e). In general, the climate sensitivity S has to be corrected for all slow feedback processes to determine S^a [Rohling *et al.*, 2012]. In this simple model there are no slow feedbacks other than the land-ice albedo feedback present that could cause such differences/uncertainties in the climate sensitivities. Hence, the different values of the climate sensitivity must be the model’s expression of state dependency of the fast feedback, here the sea ice feedback. In fact, in our model a large amount of sea ice disappears within a few decades from the glacial simulation with $2 \times \text{CO}_2$ (Figure 1d), confirming the assumption of sea ice being a fast feedback. In the interglacial simulation, however, there is much less sea ice present, and therefore, though fast, the strength of this feedback is different from results starting from the glacial background climate state.

Because in the model sea ice is the only fast feedback process, the radiation balance implies that the value of $S_{[\text{CO}_2, \text{LI}, \text{SI}]}$ (where sea ice is considered as forcing) must be close to the so-called Planck climate sensitivity $S_0 = 1/(4\varepsilon\sigma_B T_E^3)$, with ε the emissivity of the atmosphere, σ_B the Stefan-Boltzmann constant, and T_E the average equilibrium temperature of Earth’s surface. Indeed, $S_{[\text{CO}_2, \text{LI}, \text{SI}]}$ is very close to $0.3 \text{ K (W m}^{-2}\text{)}^{-1}$ and slightly different for glacial and interglacial initial states, because not all simulations are in equilibrium. The atmosphere-ocean heat exchange acts on a time scale in between slow and fast feedbacks, and therefore, the radiation budget is slightly out of balance in the $2 \times \text{CO}_2$ experiments.

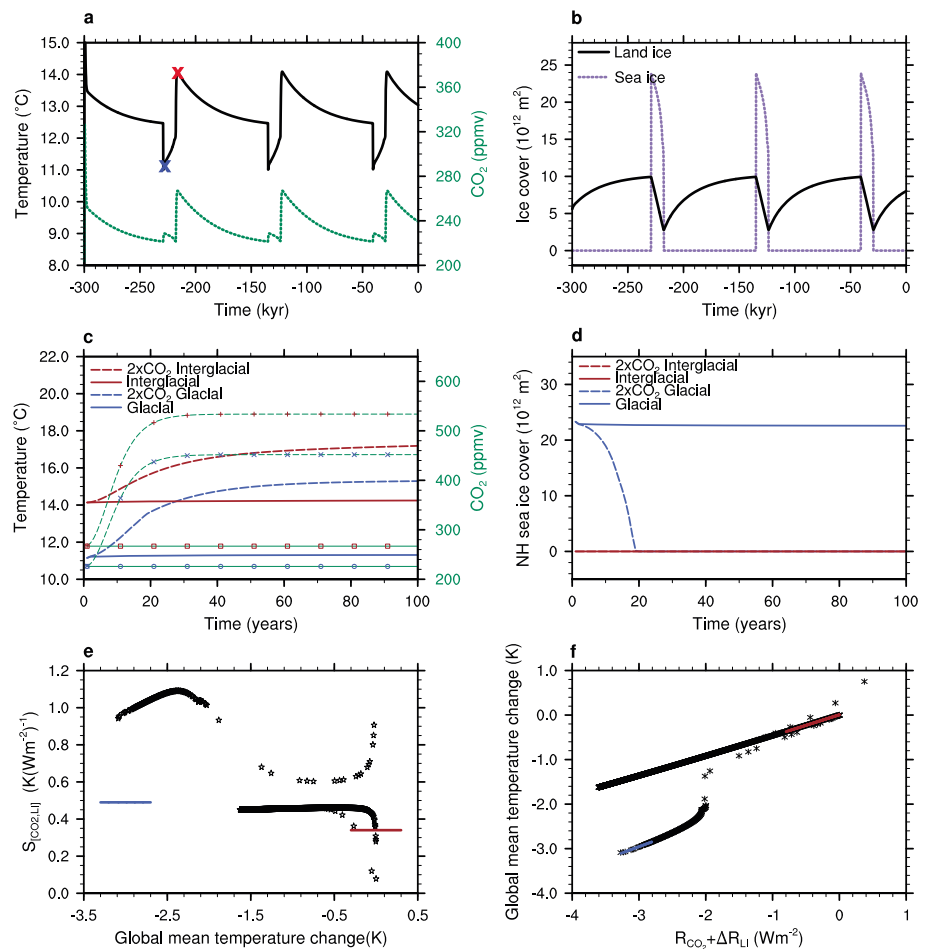


Figure 1. Climate sensitivity based on the conceptual climate model. (a) Global mean surface temperature (GMST) (black line) and atmospheric CO₂ (green line) as simulated by the box model as a function of time; red (blue) cross marks the reference temperature for an interglacial (glacial); (b) land- (solid black line) and sea ice (dashed purple line) cover in the northern polar box as a function of time; (c) quasi-equilibrium simulations (100 years) with prescribed CO₂. Thick red (blue) lines show GMST in simulations starting from an interglacial (glacial) state; solid lines show simulations with constant atmospheric CO₂ (shown as thin green lines with blue and red symbols for a glacial or interglacial state, respectively), while dashed lines show simulations in which the atmospheric CO₂ level is doubled within the first 30 years of simulation (shown as thin green dashed lines with blue and red symbols); (d) Northern Hemisphere sea-ice cover for the 100 year quasi-simulations, red (blue) lines mark simulations starting from an interglacial (glacial) state, solid (dashed) lines mark simulations with constant (doubling) CO₂ level as in Figure 1c; (e) specific climate sensitivity $S_{[CO_2,LI]}$ calculated in the traditional way with a fixed reference climate (red cross in Figure 1a); blue (red) horizontal line denotes $S_{[CO_2,LI]}$ estimated from the $2 \times CO_2$ experiments with glacial (interglacial) initial state; (f) temperature anomalies ΔT versus radiative forcing: The (local) slopes determine the state dependent specific climate sensitivities; blue (red) line indicates regression lines over the glacial (interglacial) part of the data.

When using paleorecords to determine climate sensitivity, another approach has to be taken: Climate states (usually separated in time quite substantially) with different temperatures, atmospheric CO₂ concentrations and land ice distributions are compared. Traditionally, this is done by estimating the differences ΔT and ΔR with respect to a fixed reference climate (e.g., the preindustrial climate). Figure 1e shows the simulated climate sensitivity determined by differences with respect to an interglacial climate (red cross in Figure 1a) from a 300 kyr glacial-interglacial simulation. Two temperature regimes appear, with higher climate sensitivity values during cold periods and lower values during warm periods, expressing the background state dependency of the fast sea-ice feedback in the model as described before. The actual value of $S_{[CO_2,LI]}$ in glacial and interglacial periods is, however, very different from the ones determined by the $2 \times CO_2$ experiments (blue and red bars in Figure 1e).

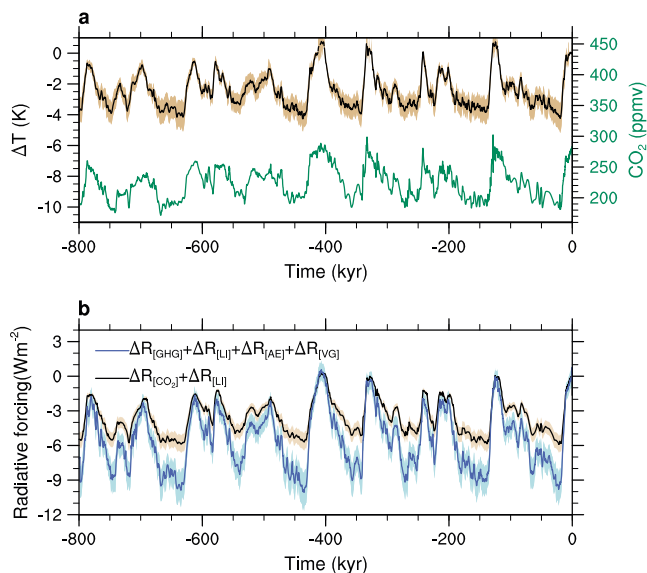


Figure 2. Data over the last 800 kyr used to estimate climate sensitivity. Shaded areas around the curves indicate uncertainty intervals ($\pm 1\sigma$); (a) global mean temperature anomalies with respect to $T^{PI} = 286.5$ K (black line) considering a global cooling at LGM of $\Delta T = -4.0$ K and CO₂ (green line) records; (b) radiative forcing due to atmospheric CO₂ and land-ice cover (black line) and due to all known and reconstructed forcings, i.e., GHG, LI, AE, and VG (blue line).

(Figure 1f) become comparable to the glacial and interglacial climate sensitivity values as determined in the $2 \times \text{CO}_2$ experiments.

In conclusion, because the fast feedbacks depend on the background climate state, climate sensitivity from paleorecords should be determined from the local slope of the ΔT versus ΔR relation. In the next section, we will apply this method to the late Pleistocene climate record.

3. Data of the Last 800 kyr

We use a compilation of several environmental records and model-based derived variables over the last 800 kyr [Köhler et al., 2010; Rohling et al., 2012]. In the following, ΔT and ΔR denote anomalies with respect to preindustrial values.

Our estimated global temperature anomalies are based on (i) the deconvolution of the benthic $\delta^{18}\text{O}$ -stack [Lisiecki and Raymo, 2005; Bintanja et al., 2005] into a Northern Hemispheric land (40° – 80°N) temperature anomaly ΔT_{NH} combined with a constant polar amplification factor $\alpha_{\text{NH}} = 3.75 \pm 0.35$ ($\pm 1\sigma$) and (ii) an Antarctic temperature anomaly ΔT_{ANT} from the EPICA Dome C data [Jouzel et al., 2007] with polar amplification factor $\alpha_{\text{ANT}} = 2.25 \pm 0.25$, to match the most recent global mean temperature reconstruction at LGM of -4.0 K [Annan and Hargreaves, 2013] by $\Delta T = (\frac{\Delta T_{\text{NH}}}{\alpha_{\text{NH}}} + \frac{\Delta T_{\text{ANT}}}{\alpha_{\text{ANT}}})/2$ (Figure 2a). The resulting polar amplification factors are high compared to climate model results [Masson-Delmotte et al., 2006; Mahlstein and Knutti, 2012]. In Text S1 in the supporting information, a similar analysis as below is shown but then based on the LGM temperature reconstruction by Schneider von Deimling et al. [2006] and a polar amplification factor of $\alpha = 2.75$, which is closer to model estimates of polar amplification [Masson-Delmotte et al., 2006]. The CO₂ reconstruction [Petit et al., 1999; Monnin et al., 2001; Siegenthaler et al., 2005; Lüthi et al., 2008] (Figure 2a) is used to calculate radiative forcing changes due to CO₂ [Myhre et al., 1998]. Radiative forcing changes due to albedo of land-ice coverage are calculated from the land-ice area reconstructions [Bintanja et al., 2005] in line with Rohling et al. [2012]. Our data set contains uncertainties of all variables as estimated previously by Köhler et al. [2010] and Rohling et al. [2012] (shown as shaded bands in Figure 2) and is interpolated to 100 year time steps. Uncertainties are given as mean $\pm 1\sigma$ (standard deviation). As the temperature and polar amplification factors, the radiative forcing data may also have uncertainties, which are not included and

More precisely, according to equation (2), $S_{[\text{CO}_2, \text{LI}]}$ (in the model approximating S^σ) is the slope in a graph showing T versus $(R_{[\text{CO}_2]} + \Delta R_{[\text{LI}]})$ as shown in Figure 1f. Under the assumption of no state dependency, a linear relation between ΔT and $(\Delta R_{[\text{CO}_2]} + \Delta R_{[\text{LI}]})$ is expected, i.e., with a constant slope. The two regimes visible in Figure 1f (black symbols) with different (local) slopes are an expression of the fact that the fast feedbacks depend on the background climate state. Again, S^σ is generally higher for cold climates than for warm climates. At the discontinuous point close to $\Delta R_{[\text{CO}_2]} + \Delta R_{[\text{LI}]} \approx -2 \text{ W m}^{-2}$ (the models glacial-interglacial transition), the local slope is even undefined or very large. Such large variations do not appear in Figure 1e when S^σ is determined from differences with respect to a fixed reference climate. Moreover, the slopes at the cold and warm ends of the relation

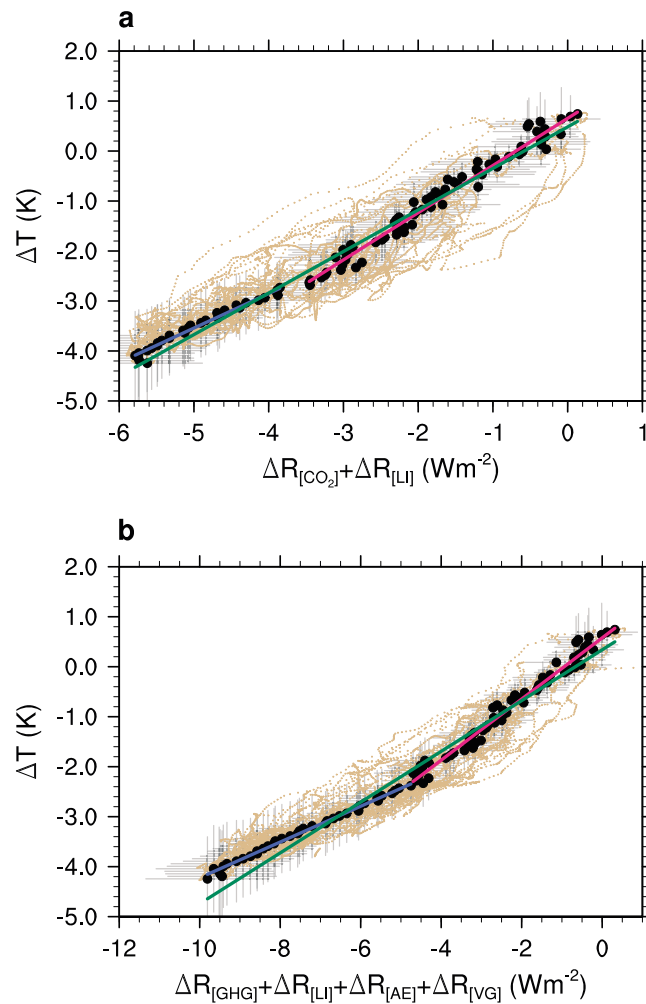


Figure 3. Climate sensitivity based on 800 kyr of data. (a) Temperature anomaly considering a global cooling at LGM of $\Delta T = -4.0$ K versus $\Delta R_{[CO_2]} + \Delta R_{[LI]}$; (b) temperature anomaly versus $\Delta R_{[GHG]} + \Delta R_{[LI]} + \Delta R_{[AE]} + \Delta R_{[VG]}$; light dots indicate all data points, black thick dots represent the data set divided into 100 temperature bins (bin size ≈ 0.05 K) with horizontal and vertical lines denoting the uncertainty limits ($\pm 1\sigma$) for each point; linear regressions on the binned data using all points (green), only warm data (red) and only cold data (blue), respectively, are calculated. See text for how the breakpoint between warm and cold data is determined.

In Figure 3 the temperature anomalies are shown versus the radiative perturbations. To determine the (local) slope between temperature and radiative forcing, the data set is divided into $N = 100$ equally spaced temperature bins (black dots in Figure 3 show the bin average together with its uncertainty). The binning is necessary because for cold periods (such as the LGM), there are much more data available than for the warm periods. In the following regression analysis, however, all temperature regimes have the same weight. Without binning, the analysis leads, however, to very similar results for $S_{[GHG,LI,AE,VG]}$, while for $S_{[CO_2,LI]}$ the oversampling of the cold periods has a larger impact. The uncertainty in both ΔR_n and ΔT_n for each bin is estimated as the maximum of two values: (i) the arithmetic mean of the variances of all individual data points in that bin, i.e.,

$$\sigma_0(\Delta R_n) = \sqrt{\frac{1}{K_n} \sum_{k=1}^{K_n} \Delta R_k^2}, \quad (3)$$

difficult to estimate. For example, the radiative forcing $\Delta R_{[LI]}$ is calculated from reconstructions of land ice area using a constant difference between the albedo of land ice and ice-free land (tundra) [Köhler *et al.*, 2010]. Different values for these two albedos might affect the $\Delta R_{[LI]}$ in a systematic way and therefore also impact the estimate of the climate sensitivity.

The temperature record together with the radiative forcing changes due to CO_2 and reconstructed land-ice albedo variations (Figure 2) allows calculating the specific sensitivities $S_{[CO_2]}$ and $S_{[CO_2,LI]}$. In the traditional way, with a fixed reference climate, i.e., the preindustrial climate, we find values $S_{[CO_2]} = 2.05 \pm 0.75 \text{ K (W m}^{-2}\text{)}^{-1}$ and $S_{[CO_2,LI]} = 0.70 \pm 0.18 \text{ K (W m}^{-2}\text{)}^{-1}$ from the complete data set. The latter is similar to results from a model ensemble for the LGM [Hargreaves *et al.*, 2012]. In the real climate system, the land-ice albedo feedback is not the only slow feedback, and therefore, $S_{[CO_2,LI]}$ is only an approximation of S^a . Other factors such as dust, vegetation distributions, or greenhouse gases other than CO_2 , e.g., CH_4 or N_2O need to be accounted for. From the data over the last 800 kyr, the closest approximation of S^a that can be estimated is $S_{[GHG,LI,AE,VG]}$ including the radiative forcing due to greenhouse gases from ice cores CO_2 , CH_4 , and N_2O (GHG), land ice (LI), aerosols (AE), and vegetation cover (VG) as estimated in Köhler *et al.* [2010] (Figure 2b).

Table 1. Overview of $S_{[CO_2,LI]}$ and $S_{[GHG,LI,AE,VG]}$ ($K (W m^{-2})^{-1}$) Calculated From Data of the Last 800 kyr Depending on Whether or Not the Background Climate State of the Fast Feedbacks Are Considered and on How Temperature Time Series Are Normalized to Fit Reconstructed Global Cooling at LGM (ΔT_{LGM})^a

$\Delta T_{LGM} = -4.0 \pm 0.8 \text{ K [Annan and Hargreaves, 2013]}$						
	$S_{[CO_2,LI]}$			$S_{[GHG,LI,AE,VG]}$		
ΔT range (K)	-4.3–0.8 (all)	-4.3 to -2.7 (cold)	-2.7–0.8 (warm)	-4.3–0.8 (all)	-4.3 to -2.7 (cold)	-2.7–0.8 (warm)
$S \pm \sigma(S)$ ($K (W m^{-2})^{-1}$)	0.83 ± 0.05	0.69 ± 0.24	0.94 ± 0.1	0.51 ± 0.03	0.36 ± 0.08	0.61 ± 0.07
	(green line in Figure 3a)	(blue line in Figure 3a)	(red line in Figure 3a)	(green line Figure 3b)	(blue line Figure 3b)	(red line Figure 3b)
$\Delta T^0 \pm \sigma(\Delta T^0)$ (K)	0.48 ± 0.14	-0.09 ± 1.18	0.65 ± 0.20	0.34 ± 0.12	-0.64 ± 0.58	0.58 ± 0.19
r^2	0.98	0.97	0.98	0.98	0.99	0.98
S previous study	0.74 ± 0.28			0.47 ± 0.17		
$\Delta T_{LGM} = -4.0... -5.8 \text{ K [Annan and Hargreaves, 2013; Schneider von Deimling et al., 2006]}$						
S range ($K (W m^{-2})^{-1}$)	0.78–1.24	0.45–1.25	0.84–1.46	0.48–0.75	0.28–0.60	0.54–0.95

^aWe use the most recent extensive reconstruction of the LGM climate by Annan and Hargreaves [2013] as standard. The spread in values is assessed by using one other reconstruction indicating a considerably stronger LGM cooling of -5.8 K [Schneider von Deimling et al., 2006].

and (ii) the spread of values within one bin as standard deviation

$$\sigma_1(\Delta R_n) = \sqrt{\frac{1}{K_n} \sum_{k=1}^{K_n} (R_k - \bar{R}_n)^2} \tag{4}$$

For temperature, $\sigma_1(\Delta T_n)$ is very small as is the bin size, but for the radiative perturbation, $\sigma_1(\Delta R_n)$ might be larger than $\sigma_0(\Delta R_n)$. From this binned data set we estimate a (locally) linear relationship between the temperature anomaly ΔT and the radiative perturbation ΔR :

$$\Delta T = \Delta T^0 + S \cdot \Delta R, \tag{5}$$

with the ΔT^0 as y axis intercept and the climate sensitivity S as slope.

The (local) slopes are determined using linear regression accounting for errors in both the predictand ($\Delta R_{[X]}$) and the dependent variable (ΔT) [Press, 1992]. A merit function weighted with the uncertainties is minimized, and regression parameters (y axis intercept and slope) are returned together with their uncertainties. For each linear regression, we determine the coefficient of determination r^2 to assess the explained variance of the fit, see Table 1.

Initially, we perform the regression analysis on the complete binned data set, i.e., we assume no state dependency. Alternatively, the data set is divided into two parts, and for each part the same linear regression analysis is applied. The sum of the two squared residuals is minimized in order to find the optimal breakpoint [Easterling and Peterson, 1995]. At this breakpoint we test the significance of the two-phase fit by using a likelihood statistic as in Easterling and Peterson [1995] based on the squared residuals of one fit to the whole data set and the squared residuals of the two separate fits. In all cases an F -test reveals that breaking up the data set into two parts yields a statistically significant better fit to the data than only one regression line. Finally, the slopes of the two individual regression lines are in all cases significantly different from each other and from the one-fit regression slope using a Student's t test at the 95% significance level. The result of the linear regression analysis is that taking into account state dependency by dividing the data set in two parts yields generally lower values for the climate sensitivity during cold (glacial) periods than during warm intervals (Table 1). In the conceptual model of section 2, the dominating fast feedback is the sea ice-albedo feedback, which tends to be stronger during cold periods and therefore leads to higher climate sensitivity during glacial periods. Previous model studies have suggested that not only the sea-ice albedo feedback [Ritz et al., 2011] but also the short-wave cloud feedbacks [Crucifix, 2006; Hargreaves et al., 2007] or the water vapor and lapse-rate feedbacks [Yoshimori et al., 2011] are temperature dependent. Our results here suggest that these other fast feedbacks, which promote a higher sensitivity in warm climates, are apparently stronger than the sea ice-albedo feedback. The sea ice-albedo feedback is less effective in warm climates with little or no sea ice changes, and the water vapor feedback is stronger when there is more moisture in

the atmosphere, i.e., in a warm climate with enhanced hydrological cycle. To disentangle the contributions of individual feedbacks from the observations, accurate reconstructions of sea ice, aerosols, clouds, and other fast feedbacks are needed. Alternatively, climate models run for at least a few glacial-interglacial cycles could be used to estimate these contributions.

4. Discussion and Conclusions

Using the local slope of the relation between temperature anomalies and radiative forcing and assuming that land ice provides the dominant slow feedback, we estimate the specific sensitivity $S_{[\text{CO}_2, \text{LI}]} = 0.94 \pm 0.10 \text{ K (W m}^{-2}\text{)}^{-1}$ for global mean temperature anomalies between -2.7 and $+0.8 \text{ K}$. This value is higher than a previous estimate $S_{[\text{CO}_2, \text{LI}]} = 0.74 \pm 0.28 \text{ K (W m}^{-2}\text{)}^{-1}$ (scaled to the LGM temperature reconstruction as used here) based on the same radiative forcing data [Rohling *et al.*, 2012] but neglecting the state dependency of the fast feedbacks.

Considering all available forcings, the Charney climate sensitivity S^a should be approximated by $S_{[\text{GHG}, \text{LI}, \text{AE}, \text{VG}]}$, which we estimate to be $0.61 \pm 0.07 \text{ K (W m}^{-2}\text{)}^{-1}$ for warm climates. Our estimate of S^a , however, strongly depends on the scaling of the temperature record to match the most recent reconstruction of LGM cooling [Annan and Hargreaves, 2013] and consequently on the temperature reconstruction quality. An earlier estimate by Schneider von Deimling *et al.* [2006] suggests an LGM cooling of $-5.8 \pm 1.4 \text{ K}$, which leads in our analysis to $S^a = 0.87 \pm 0.08 \text{ K (W m}^{-2}\text{)}^{-1}$ (Text S1). Another estimate based on one climate model and proxy data suggests even less LGM cooling than in Annan and Hargreaves [2013] of only -3.0 (90% probability range $[-1.7, 3.7] \text{ K}$, [Schmittner *et al.*, 2011]) leading in our analysis to S^a even lower than our reference case.

Several factors in our analysis, which at this stage cannot be explicitly taken into account, might influence the estimate for S^a :

1. In order to match the most recent reconstruction of global mean cooling at the LGM [Annan and Hargreaves, 2013], we assumed time-independent polar amplification factors for the Southern and Northern Hemispheres [Singarayer and Valdes, 2010; Masson-Delmotte *et al.*, 2006]. Although their uncertainty estimates partly account for a possible time dependency, more information on the relation between high latitude and global mean temperatures is necessary.
2. Similarly as the LGM temperature, the radiative forcing reconstructions might be subject to systematic uncertainties. Using a higher temperature difference ΔT_{LGM} in our analysis leads to different slopes (climate sensitivities) for warm and cold periods, while the breakpoint is not significantly affected. With a nonconstant (over time) systematic error in either ΔT or ΔR , the location of the breakpoint between warm and cold periods will be affected as well.
3. The efficacy of climate forcings due to varying spatial distribution of radiative forcings can vary over time, which makes it difficult to directly compare the future double CO_2 experiments with glacial climate forcing [Hansen *et al.*, 2005].
4. Orbital forcing varies over time, and while the varying insolation has been included in the analysis, we did not take into account the dependency of the fast feedbacks on the solar insolation. However, in a previous study [Köhler *et al.*, 2010] it was shown for the sea-ice albedo feedback, that the impact of sea-ice area changes between glacial and interglacial states is much larger than the effect of local insolation changes.
5. The equilibrium concept of climate sensitivity might not be adequate in the presence of climate variations on millennial time scales such as the large and rapid changes during Dansgaard-Oeschger events which are believed to be caused by nonlinear processes in the climate system [Schulz, 2002; Ganopolski and Rahmstorf, 2002; Ditlevsen and Ditlevsen 2009]. For our data set the equilibrium assumption has been tested [Rohling *et al.*, 2012; Köhler *et al.*, 2010] and excluding data points from quickly varying periods did not strongly affect the results.

There are three ways to further improve the estimate of S^a from paleoclimate data:

1. Extend the analysis on how climate sensitivity depends on temperature to a wider range by including past reconstructions of warmer climates (e.g., Pliocene). Indeed, a limitation of the analysis is that our results are based on data of mostly colder than present climate.
2. Add more information on the different feedback processes and their dependency on the global mean temperature contributing to the combined feedback parameter by improved reconstructions.

3. Improve the temperature reconstructions. For the late Pleistocene including the LGM, the uncertainties in ΔT are still large, in particular, for the land-ocean temperature differences and meridional temperature gradients.

In summary, we have provided a novel method to estimate the equilibrium climate sensitivity S^{α} from a paleo-data set explicitly accounting for a possible state dependency of the fast feedbacks and we show that taking this state dependency into account strongly affects the outcome of the results. From data (and model-based interpretation) covering the last 800 kyr, we estimate $S^{\alpha} = 0.61 \pm 0.07 \text{ K (W m}^{-2}\text{)}^{-1}$ (given the latest LGM cooling reconstruction of -4.0 K) valid for global mean temperatures between 2.3 K colder and 0.8 K warmer than the preindustrial climate. Due to the large uncertainty of LGM temperature reconstructions, this value may be higher up to $S^{\alpha}_{\Delta T_{\text{LGM}}=-5.8\text{K}} = 0.87 \pm 0.08 \text{ K (W m}^{-2}\text{)}^{-1}$. Combined, this corresponds to an equilibrium global mean surface warming of 2.0–3.5 K for $2 \times \text{CO}_2$. For climate states more than 2.3 K colder than the preindustrial climate, we find $S^{\alpha} = 0.28\text{--}0.6 \text{ K (W m}^{-2}\text{)}^{-1}$, which is 60% smaller than that for the warmer conditions. These estimates can be further improved if more accurate temperature reconstructions and better estimates of radiative forcing due to slow feedbacks become available.

Acknowledgments

The analysis of the data-based changes in climate sensitivity for the last 800 kyr used the following public available data sets from the NOAA National Climatic Data Center (<http://www.ncdc.noaa.gov/paleo/paleo.html>). This paper contributes to the gravity program, *Reading the past to project the future*, funded by the Netherlands Organisation for Scientific Research (NWO).

The Editor thanks Michel Crucifix and an anonymous reviewer for their assistance in evaluating this paper.

References

- Andrews, T., and P. M. Forster (2008), CO₂ forcing induces semi-direct effects with consequences for climate feedback interpretations, *Geophys. Res. Lett.*, *35*, L04802, doi:10.1029/2007GL032273.
- Annan, J. D., and J. C. Hargreaves (2013), A new global reconstruction of temperature changes at the Last Glacial Maximum, *Clim. Past*, *9*, 367–376, doi:10.5194/cp-9-367-2013.
- Bintanja, R., R. S. W. van de Wal, and J. Oerlemans (2005), Modelled atmospheric temperatures and global sea levels over the past million years, *Nature*, *437*, 125–128.
- Charney, J. G. (1979), *Carbon Dioxide and Climate: A Scientific Assessment*, National Acad. of Science, Washington, D. C.
- Crucifix, M. (2006), Does the Last Glacial Maximum constrain climate sensitivity?, *Geophys. Res. Lett.*, *33*(18), L18701, doi:10.1029/2006GL027137.
- Ditlevsen, P. D., and O. D. Ditlevsen (2009), On the stochastic nature of the rapid climate shifts during the last ice age, *J. Clim.*, *22*, 446–457, doi:10.1175/2008jcli2430.1.
- Easterling, D. R., and T. C. Peterson (1995), A new method for detecting undocumented discontinuities in climatological time series, *Int. J. Climatol.*, *15*(4), 369–377, doi:10.1002/joc.3370150403.
- Ganopolski, A., and S. Rahmstorf (2002), Abrupt glacial climate change due to stochastic resonance, *Phys. Rev. Lett.*, *88*(3), 038501, doi:10.1103/PhysRevLett.88.038501.
- Gildor, H., and E. Tziperman (2001), A sea ice climate switch mechanism for the 100-kyr glacial cycles, *J. Geophys. Res.*, *106*(C5), 9117–9133.
- Gildor, H., E. Tziperman, and J. R. Toggweiler (2002), Sea ice switch mechanism and glacial-interglacial CO₂ variations, *Global Biogeochem. Cycles*, *16*(3), 1032, doi:10.1029/2001GB001446.
- Hansen, J., et al. (2005), Efficacy of climate forcings, *J. Geophys. Res.*, *110*, D18104, doi:10.1029/2005JD005776.
- Hargreaves, J. C., A. Abe-Ouchi, and J. D. Annan (2007), Linking glacial and future climates through an ensemble of GCM simulations, *Clim. Past*, *3*, 77–87.
- Hargreaves, J. C., J. D. Annan, M. Yoshimori, and A. Abe-Ouchi (2012), Can the last glacial maximum constrain climate sensitivity?, *Geophys. Res. Lett.*, *39*, L24702, doi:10.1029/2012GL053872.
- Jouzel, J., et al. (2007), Orbital and millennial Antarctic climate variability over the past 800,000 years, *Science*, *317*(5839), 793–796.
- Knutti, R., and G. C. Hegerl (2008), The equilibrium sensitivity of the Earth's temperature to radiation changes, *Nat. Geosci.*, *1*(11), 735–743, doi:10.1038/ngeo337.
- Köhler, P., R. Bintanja, H. Fischer, F. Joos, R. Knutti, G. Lohmann, and V. Masson-Delmotte (2010), What caused Earth's temperature variations during the last 800,000 years? Data-based evidence on radiative forcing and constraints on climate sensitivity, *Quat. Sci. Rev.*, *29*, 129–145, doi:10.1016/j.quascirev.2009.09.026.
- Lisiecki, L. E., and M. E. Raymo (2005), A Pliocene-Pleistocene stack of 57 globally distributed benthic $\delta^{18}\text{O}$ records, *Paleoceanography*, *20*, PA1003, doi:10.1029/2004PA001071.
- Lüthi, D., et al. (2008), High-resolution CO₂ concentration record 650,000–800,000 years before present, *Nature*, *453*, 379–382, doi:10.1038/nature06949.
- Mahlstein, I., and R. Knutti (2012), September Arctic sea ice predicted to disappear near 2°C global warming above present, *J. Geophys. Res.*, *117*, D06104, doi:10.1029/2011JD016709.
- Masson-Delmotte, V., et al. (2006), Past and future polar amplification of climate change: Climate model intercomparisons and ice-core constraints, *Clim. Dyn.*, *26*(5), 513–529, doi:10.1007/s00382-005-0081-9.
- Monnin, E., A. Indermühle, A. Dällenbach, J. Flückiger, B. Stauffer, T. Stocker, D. Raynaud, and J.-M. Barnola (2001), Atmospheric CO₂ concentrations over the last glacial termination, *Science*, *291*, 112–114.
- Myhre, G., E. J. Highwood, K. P. Shine, and F. Stordal (1998), New estimates of radiative forcing due to well mixed greenhouse gases, *Geophys. Res. Lett.*, *25*(14), 2715–2718, doi:10.1029/98GL01908.
- Petit, J., et al. (1999), Climate and atmospheric history of the past 420,000 years from the Vostok ice core, Antarctica, *Nature*, *399*(429–436).
- Press, W. H. (1992), *Numerical Recipes in FORTRAN: The Art of Scientific Computing*, Cambridge Univ. Press, New York.
- Ritz, S. P., T. F. Stocker, and F. Joos (2011), A coupled dynamical ocean-energy balance atmosphere model for paleoclimate studies, *J. Clim.*, *24*(2), 349–375.
- Rohling, E. J., A. Sluijs, H. A. Dijkstra, P. Köhler, R. S. W. van de Wal, A. S. von der Heydt, and P. P. Members (2012), Making sense of palaeoclimate sensitivity, *Nature*, *491*(7426), 683–691.
- Schmittner, A., N. M. Urban, J. D. Shakun, N. M. Mahowald, P. U. Clark, P. J. Bartlein, A. C. Mix, and A. Rosell-Melé (2011), Climate sensitivity estimated from temperature reconstructions of the Last Glacial Maximum, *Science*, *334*(6061), 1385–1388, doi:10.1126/science.1203513.

- Schneider von Deimling, T., A. Ganopolski, H. Held, and S. Rahmstorf (2006), How cold was the Last Glacial Maximum?, *Geophys. Res. Lett.*, 33, L14709, doi:10.1029/2006GL026484.
- Schulz, M. (2002), The tempo of climate change during Dansgaard-Oeschger interstadials and its potential to affect the manifestation of the 1470-year climate cycle, *Geophys. Res. Lett.*, 29(1), 1002, doi:10.1029/2001GL013277.
- Senior, C. A., and J. F. B. Mitchell (2000), The time dependence of climate sensitivity, *Geophys. Res. Lett.*, 27(17), 2685–2688, doi:10.1029/2000GL011373.
- Siegenthaler, U., et al. (2005), Stable carbon cycle–climate relationship during the late Pleistocene, *Science*, 310, 1313–1317, doi:10.1126/science.1120130.
- Singarayer, J. S., and P. J. Valdes (2010), High-latitude climate sensitivity to ice-sheet forcing over the last 120 kyr, *Quat. Sci. Rev.*, 29(1-2), 43–55, doi:10.1016/j.quascirev.2009.10.011.
- Vial, J., J.-L. Dufresne, and S. Bony (2013), On the interpretation of inter-model spread in CMIP5 climate sensitivity estimates, *Clim. Dyn.*, 41(11-12), 3339–3362, doi:10.1007/s00382-013-1725-9.
- Yoshimori, M., J. C. Hargreaves, J. D. Annan, T. Yokohata, and A. Abe-Ouchi (2011), Dependency of feedbacks on forcing and climate state in physics parameter ensembles, *J. Clim.*, 24(24), 6440–6455, doi:10.1175/2011JCLI3954.1.

Supporting Information to

On the state dependency of fast feedback processes in

(palaeo) climate sensitivity

A. S. von der Heydt, P. Köhler, R. S. W. van de Wal, and H. A. Dijkstra

August 18, 2014

S1. Theoretical framework to calculate climate sensitivity from the climate model

The climate sensitivity is determined from the energy balance of the Earth. For the conceptual model *Gildor and Tziperman* (2001), we can explicitly write the energy balance of the atmosphere and extract the different contributions to climate sensitivity. Averaged over all atmospheric boxes of the model the global mean temperature T (vertically averaged) is determined by the difference between the heat flux at the top of the atmosphere F_{top} and at the surface $F_{surface}$, following the equation:

$$\frac{\partial T}{\partial t} = \frac{2^{R/C_p} g}{P_0 C_p} [(F_{top} - F_{surface})] \quad (\text{S1})$$

$$= \frac{2^{R/C_p} g}{P_0 C_p} [(H_{in} - H_{out} + R_{[surf]})], \quad (\text{S2})$$

where

$$H_{in} = (1 - \alpha_{surf})(1 - \alpha_C)(1 - q_{in}^{seaice})Q_{Solar} \quad (\text{S3})$$

$$H_{out} = \left(\varepsilon - \kappa \ln \left(\frac{\text{CO}_2}{\text{CO}_{2,ref}} \right) \right) \sigma_B T^4, \quad (\text{S4})$$

are the incoming and outgoing radiation terms at the top of the atmosphere, respectively. (R is the gas constant for dry air, C_p is the specific heat of the atmosphere at a constant pressure, P_0 a reference pressure, σ_B the Stefan Boltzmann constant and g the gravitational acceleration.) The incoming solar radiation Q_{Solar} is reduced by a constant cloud albedo term α_C and a part q_{in}^{seaice} that is directly used to melt sea ice. Where sea ice exists, 15% of the incoming shortwave radiation

is used to melt sea ice and does not enter the radiation balance of the atmosphere *Gildor et al.* (2002). α_{surf} is the surface albedo of the planet and is determined from the average albedo in each box α_{surf}^i by the fraction of sea ice, land ice, land surface and ocean surface in that box:

$$\alpha_{surf}^i = f_L^i(1 - f_{LI}^i)\alpha_L + f_L^i f_{LI}^i \alpha_{LI} + f_O^i(1 - f_{SI}^i)\alpha_O + f_O^i f_{SI}^i \alpha_{SI} \quad (\text{S5})$$

Here, f_L , f_{LI} , f_O , f_{SI} correspond to the fraction of land, land ice, ocean and sea ice, respectively, and α_L , α_{LI} , α_O , α_{SI} to the corresponding albedos of each surface type. The outgoing radiation depends on a mean emissivity of the planet ε and a term depending on the atmospheric CO₂ concentration. Here κ is chosen *Gildor et al.* (2002) such that a doubling of CO₂ will cause a radiative forcing of 4 Wm⁻². The radiation balance of the atmosphere is complemented by the radiation at the Earth's surface $R_{[surf]}$, which is in this model equal to the ocean-atmosphere heat exchange.

To access the contributions of the different forcings and feedbacks to the radiation balance, we split the global mean radiation terms into the different components due to solar radiation ($R_{[ins]}$), land ice ($R_{[LI]}$), sea ice ($R_{[SI]}$), outgoing longwave radiation ($R_{[OLW]}$), CO₂ concentration ($R_{[CO_2]}$) and the radiation at the Earth's surface ($R_{[surf]}$):

$$\frac{\partial T}{\partial t} = \frac{2^{R/C_p} g}{P_0 C_p} [R_{[ins]} + R_{[LI]} + R_{[SI]} + R_{[OLW]} + R_{[CO_2]} + R_{[surf]}] \quad (\text{S6})$$

The different contributions to the radiation balance can be expressed as:

$$R_{[ins]} = (1 - \alpha_C) Q_{solar} \quad (\text{S7})$$

$$R_{[LI]} = R_{[ins]} \sum_i (f_L^i(1 - f_{LI}^i)\alpha_L + f_L^i f_{LI}^i \alpha_{LI})(q_{in}^{seaice} - 1) \quad (\text{S8})$$

$$R_{[SI]} = -R_{[ins]} \sum_i [q_{in}^{seaice} + (1 - q_{in}^{seaice})(f_O^i(1 - f_{SI}^i)\alpha_O + f_O^i f_{SI}^i \alpha_{SI})] \quad (\text{S9})$$

$$R_{[OLW]} = -\sum_i \varepsilon_i \sigma_B T_i^4 \quad (\text{S10})$$

$$R_{[CO_2]} = \sum_i \kappa \ln \frac{pCO_2}{pCO_{2,ref}} \sigma_B T_i^4 \quad (\text{S11})$$

$$R_{[surf]} = -\sum_i Q_{oa}^i. \quad (\text{S12})$$

When comparing two equilibrium climate states with global mean temperatures T_1 and T_2 (and $\Delta T = T_2 - T_1$), the radiation balance Eq.S6 reads:

$$0 = \Delta R_{[ins]} + \Delta R_{[LI]} + \Delta R_{[SI]} + \Delta R_{[OLW]} + \Delta R_{[CO_2]} + \Delta R_{[surf]}. \quad (\text{S13})$$

The different contributions to the radiative balance are shown in Supplementary Fig. S1. As we consider constant solar radiation and no changes in cloud albedo, $\Delta R_{[ins]} = 0$, and, when we put

all the forcing or slow feedbacks on the left hand side and all fast feedback processes on the right hand side, we obtain:

$$\Delta R_{[\text{CO}_2]} + \Delta R_{[LI]} = -\Delta R_{[OLW]} - \Delta R_{[SI]} - \Delta R_{[surf]}. \quad (\text{S14})$$

This finally leads to the expressions for the specific climate sensitivities

$$S_{[\text{CO}_2]} = \frac{\Delta T}{\Delta R_{[\text{CO}_2]}} = \frac{-\Delta T}{\Delta R_{[OLW]} + \Delta R_{[SI]} + \Delta R_{[surf]} + \Delta R_{[LI]}} \quad (\text{S15})$$

$$S_{[\text{CO}_2, LI]} = \frac{\Delta T}{\Delta R_{[\text{CO}_2]} + \Delta R_{[LI]}} = \frac{-\Delta T}{\Delta R_{[OLW]} + \Delta R_{[SI]} + \Delta R_{[surf]}} \quad (\text{S16})$$

$$S_{[\text{CO}_2, LI, SI]} = \frac{\Delta T}{\Delta R_{[\text{CO}_2]} + \Delta R_{[LI]} + \Delta R_{[SI]}} = \frac{-\Delta T}{\Delta R_{[OLW]} + \Delta R_{[surf]}}. \quad (\text{S17})$$

The last expression should approximate the sensitivity without feedbacks (i.e. only Planck feedback), $S_0 = (-4\varepsilon\sigma_B T^3)^{-1} \simeq 0.3 \text{ K (W m}^{-2}\text{)}^{-1}$. In the model there is, however, one more radiation term due to the atmosphere-ocean heat exchange (ΔR_{surf}), which acts on fast to intermediate time scales. Therefore, $S_{[\text{CO}_2, LI, SI]}$ still slightly deviates from the Planck sensitivity.

S2. Charney climate sensitivity from a different LGM temperature reconstruction

As mentioned in the main text, reconstructions of both temperature and radiative forcing changes have a large uncertainty. Here we explore the influence of using a different temperature record in the analysis of the climate sensitivity and its state dependency. The most recent approach *Annan and Hargreaves* (2013) calculates a cooling of $-4.0 \pm 0.8 \text{ K}$ (with 95% CI). Earlier reconstructions for the LGM based on data and a climate model found a cooling of $-5.8 \pm 1.4 \text{ K}$ *Schneider von Deimling et al.* (2006). Here we perform the same analysis for determining the climate sensitivity from the local slopes with the temperature record scaled to match this LGM temperature reconstruction.

To match the stronger cooling for the LGM as found in *Schneider von Deimling et al.* (2006), the temperature record *Bintanja et al.* (2005) for the northern hemisphere high-latitude temperature was scaled *Köhler et al.* (2010) by a (constant) polar amplification factor of 2.75. The climate sensitivity analysis as was done in the main text with this different temperature record is shown in Fig. S2 (regression values are given in Table S2 and Table 1 of the main text). We find the same trends for the specific climate sensitivities $S_{[\text{CO}_2, LI]}$ and $S_{[GHG, LI, AE, VGI]}$ with lower values during cold (glacial) periods, however, the values of the climate sensitivity are systematically higher than for the most recent reconstruction *Annan and Hargreaves* (2013).

The very weak LGM cooling as found in *Schmittner et al.* (2011) can be achieved by scaling northern and southern hemisphere temperature records as used in the main text by very high polar

amplification factors $\alpha_{NH} = 5$ and $\alpha_{ANT} = 3$. The climate sensitivity analysis as was done in the main text with this different temperature record leads again to the same trends for the specific climate sensitivities with systematically lower values.

Supplementary References

- Annan, J. D., and J. C. Hargreaves (2013), A new global reconstruction of temperature changes at the Last Glacial Maximum, *Clim. Past*, *9*, 367–376, doi:10.5194/cp-9-367-2013.
- Bintanja, R., R. S. W. van de Wal, and J. Oerlemans (2005), Modelled atmospheric temperatures and global sea levels over the past million years, *Nature*, *437*, 125–128.
- Gildor, H., and E. Tziperman (2000), Sea ice as the glacial cycles' climate switch: Role of seasonal and orbital forcing, *Paleoceanography*, *15*(6), 605–615.
- Gildor, H., and E. Tziperman (2001), A sea ice climate switch mechanism for the 100-kyr glacial cycles, *J. Geophys. Res.*, *106*(C5), 9117–9133.
- Gildor, H., E. Tziperman, and J. R. Toggweiler (2002), Sea ice switch mechanism and glacial-interglacial CO₂ variations, *Glob. Biogeochem. Cyc.*, *16*(3), 1032, doi:{10.1029/2001GB001446}.
- Köhler, P., R. Bintanja, H. Fischer, F. Joos, R. Knutti, G. Lohmann, and V. Masson-Delmotte (2010), What caused Earth's temperature variations during the last 800,000 years? Data-based evidence on radiative forcing and constraints on climate sensitivity, *Quat. Sci. Rev.*, *29*(1-2, Sp. Iss. SI), 129–145, doi:10.1016/j.quascirev.2009.09.026.
- Schmittner, A., N. M. Urban, J. D. Shakun, N. M. Mahowald, P. U. Clark, P. J. Bartlein, A. C. Mix, and A. Rosell-Melé (2011), Climate sensitivity estimated from temperature reconstructions of the Last Glacial Maximum, *Science*, *334*(6061), 1385–1388, doi:10.1126/science.1203513.
- Schneider von Deimling, T., A. Ganopolski, H. Held, and S. Rahmstorf (2006), How cold was the Last Glacial Maximum?, *Geophys. Res. Lett.*, *33*, L14,709, doi:10.1029/2006GL026484.

Table S1: Radiation changes and climate sensitivities derived from the comparison of different 100-year experiments (values shown are an average of the last 20 years of each simulation). (i) Left column: Difference between an interglacial control simulation (constant CO₂) and an interglacial simulation where CO₂ is doubled within the first 30 years; (ii) middle column: same as (i) but for a glacial climate state; (iii) Difference between a glacial and an interglacial control simulation with constant (but different) CO₂.

	Interglacial (2× CO ₂ -1× CO ₂)	Glacial (2× CO ₂ -1× CO ₂)	Interglacial minus Glacial
ΔT [K]	2.90	3.96	2.93
$S_{[CO_2]}$ [K (W m ⁻²) ⁻¹]	0.34	0.47	1.46
$S_{[CO_2,LI]}$ [K (W m ⁻²) ⁻¹]	0.34	0.49	0.94
$S_{[CO_2,LI,SI]}$ [K (W m ⁻²) ⁻¹]	0.32	0.30	0.32
$\Delta R_{[LI]}$ [W m ⁻²]	-0.04	-0.22	1.10
$\Delta R_{[SI]}$ [W m ⁻²]	0.61	5.23	6.00
$\Delta R_{[OLW]}$ [W m ⁻²]	-8.41	-11.45	-8.27
$\Delta R_{[CO_2]}$ [W m ⁻²]	8.60	8.35	2.00
$\Delta R_{[surf]}$ [W m ⁻²]	-0.75	-2.31	-1.40

Table S2: Results of the linear regression on the binned data sets for a different estimate of LGM cooling (*Schneider von Deimling et al., 2006*).

$\Delta T_{\text{LGM}} = -5.8 \pm 1.4 \text{ K}$ (<i>Schneider von Deimling et al., 2006</i>)						
	$S_{[\text{CO}_2, \text{LI}]}$			$S_{[\text{GHG}, \text{LI}, \text{AE}, \text{VG}]}$		
ΔT range considered (K)	all	cold	warm	all	cold	warm
	-6.0 – 1.1	-6.0 – -3.8	-3.8 – 1.1	-6.0 – 1.1	-6.0 – -3.2	-3.2 – 1.1
ΔT^0 (K)	0.69	-0.09	0.93	0.49	-0.91	0.84
$\sigma(\Delta T^0)$ (K)	0.18	1.37	0.25	0.15	0.66	0.24
S (K (W m ⁻²) ⁻¹)	1.18	0.98	1.34	0.72	0.51	0.87
$\sigma(S)$ (K (W m ⁻²) ⁻¹)	0.06	0.27	0.12	0.03	0.09	0.08
r^2	0.98	0.97	0.98	0.98	0.99	0.98

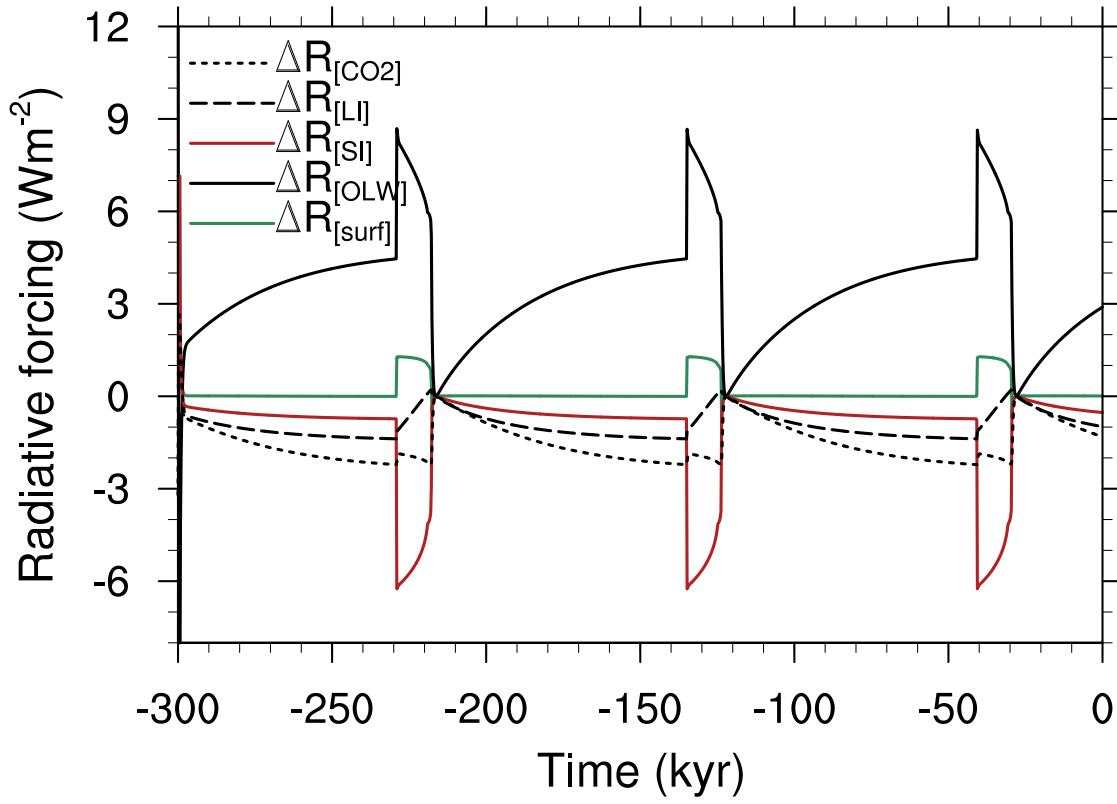


Figure S1: Different terms of the radiative balance (Eqs.S8–S12) as simulated by the climate box-model including all model components, i.e., ocean, atmosphere, sea ice, land ice, biogeochemistry as described in (Gildor and Tziperman, 2000, 2001; Gildor et al., 2002). Shown is the radiation difference with respect to an interglacial state for CO₂ (dotted line), land ice (dashed line), sea ice (red solid line), outgoing long wave radiation (black solid line) and surface heat exchange (green solid line).

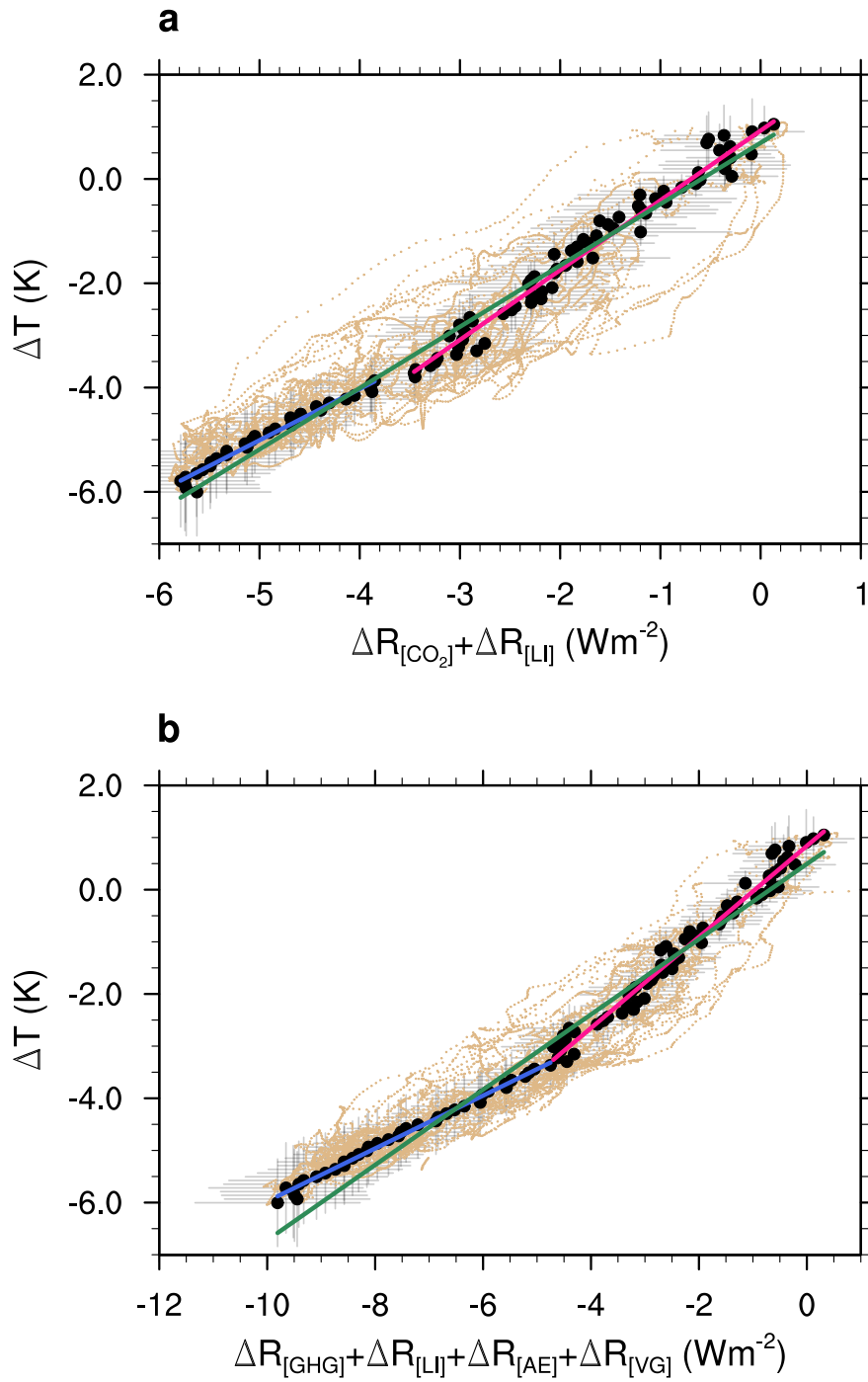


Figure S2: Climate sensitivity over the last 800 kyr based on data Köhler *et al.* (2010), with a different polar amplification factor to match the LGM cooling as reconstructed by Schneider von Deimling *et al.* (2006). (a) Temperature versus $\Delta R_{[\text{CO}_2]} + \Delta R_{[\text{LI}]}$; (b) Temperature versus $\Delta R_{[\text{GHG}]} + \Delta R_{[\text{LI}]} + \Delta R_{[\text{AE}]} + \Delta R_{[\text{VG}]}$; Light dots indicate all data points, black thick dots represent the data set divided into 100 temperature bins (bin size $\simeq 0.07$ K) with horizontal and vertical lines denoting the uncertainty limits ($\pm 1\sigma$) for each point; Straight lines indicate linear regressions on the binned data using all points (green), only warm data (red) and only cold data (blue), respectively.